CLINICAL RESEARCH

Five-Year Clinical and Functional Multislice Computed Tomography Angiographic Results After Coronary Implantation of the Fully Resorbable Polymeric Everolimus-Eluting Scaffold in Patients With De Novo Coronary Artery Disease

The ABSORB Cohort A Trial

Yoshinobu Onuma, MD,* Dariusz Dudek, MD,† Leif Thuesen, MD,‡
Mark Webster, MB CʜB,‡ Koen Nieman, MD, Pʜᴅ,*§ Hector M. Garcia-Garcia, MD, Pʜᴅ,||
John A. Ormiston, MB CʜB,¶ Patrick W. Serruys, MD, Pʜᴅ*

Rotterdam, the Netherlands; Krakow, Poland; Skejby, Denmark; and Auckland, New Zealand

Objectives This study sought to demonstrate the 5-year clinical and functional multislice computed tomography angiographic results after implantation of the fully resorbable everolimus-eluting scaffold (Absorb BVS, Abbott Vascular, Santa Clara, California).

Background Multimodality imaging of the first-in-humans trial using a ABSORB BVS scaffold demonstrated at 2 years the bioresorption of the device while preventing restenosis. However, the long-term safety and efficacy of this therapy remain to be documented.

Methods In the ABSORB cohort A trial (ABSORB Clinical Investigation, Cohort A [ABSORB A] Everolimus-Eluting Coronary Stent System Clinical Investigation), 30 patients with a single de novo coronary artery lesion were treated with the fully resorbable everolimus-eluting Absorb scaffold at 4 centers. As an optional investigation in 3 of the 4 centers, the patients underwent multislice computed tomography (MSCT) angiography at 18 months and 5 years. Acquired MSCT data were analyzed at an independent core laboratory (Cardialysis, Rotterdam, the Netherlands) for quantitative analysis of lumen dimensions and was further processed for calculation of fractional flow reserve (FFR) at another independent core laboratory (Heart Flow, Redwood City, California).

Results Five-year clinical follow-up is available for 29 patients. One patient withdrew consent after 6 months, but the vital status of this patient remains available. At 46 days, 1 patient experienced a single episode of chest pain and underwent a target lesion revascularization with a slight troponin increase after the procedure. At 5 years, the ischemia-driven major adverse cardiac event rate of 3.4% remained unchanged. Clopidogrel was discontinued in all but 1 patient. Scaffold thrombosis was not observed in any patient. Two noncardiac deaths were reported, 1 caused by duodenal perforation and the other from Hodgkin's disease. At 5 years, 18 patients underwent MSCT angiography. All scaffolds were patent, with a median minimal lumen area of 3.25 mm^2 (interquartile range: 2.20 to 4.30). Noninvasive FFR analysis was feasible in 13 of 18 scans, which yielded a median distal FFR of 0.86 (interquartile range: 0.82 to 0.94).

Conclusions The low event rate at 5 years suggests sustained safety after the implantation of a fully bioresorbable Absorb everolimus-eluting scaffold. Noninvasive assessment of the coronary artery with an option of functional assessment could be an alternative to invasive imaging after treatment of coronary narrowing with such a polymeric bioresorbable scaffold. (ABSORB Clinical Investigation, Cohort A [ABSORB A] Everolimus-Eluting Coronary Stent System Clinical Investigation [ABSORB]; NCT00300131) (J Am Coll Cardiol Intv 2013;6:999–1009) © 2013 by the American College of Cardiology Foundation

As an alternative approach to a metal drug-eluting stent, a fully bioresorbable polymeric drug-eluting device may scaffold the vessel after dilation to prevent acute closure and late constrictive remodeling, but dissolve over time to restore the native integrity of the coronary artery. Such a scaffold does not preclude surgical revascularization, and enables expansive remodeling, restores vasomotion, and is compatible with the noninvasive imaging of coronary arteries with either multislice computed tomography (MSCT) or magnetic resonance imaging (1,2).

See page 1010

Abbreviations and Acronyms

CT = computed tomography

FFR = fractional flow reserve

FFR$_{CT}$ = noninvasive fractional flow reserve according to multislice computed tomography

ID = ischemia-driven

IQR = interquartile range

IVUS = intravascular ultrasound

MACE = major adverse cardiac event(s)

MI = myocardial infarction

MSCT = multislice computed tomography

OCT = optical coherence tomography

PLLA = poly-L-lactide

PDLLA = poly-D,L-lactide

QCA = quantitative coronary angiography

TLR = target lesion revascularization

TVR = target vessel revascularization

The fully resorbable everolimus-eluting Absorb scaffold (Abbott Vascular, Santa Clara, California) was tested in the first-in-humans ABSORB (ABSORB Clinical Investigation, Cohort A [ABSORB A] Everolimus Eluting Coronary Stent System Clinical Investigation) trial enrolling 30 patients with a single de novo coronary artery lesion. Two-year imaging follow-up of the trial with multiple modality imaging can be summarized as follows (3,4): 1) bioresorption of polymeric struts (documented with intravascular ultrasonography [IVUS] and optical coherence tomography [OCT]); 2) late enlargement of the lumen from 6 months to 2 years with plaque reduction (IVUS and OCT); 3) restoration of vasomotion and endothelial function in some patients; 4) restoration of physiological cyclic (systolic and diastolic) strains; and 5) feasibility of noninvasive imaging with MSCT at 18 months (4–7). However, the long-term outcomes of biodegradation of the Absorb scaffold in human coronary arteries as well as plaque and lumen evolution beyond 2 years remains to be investigated to confirm the safety and effectiveness of the technology.

With the rapid technological advancement, cardiac MSCT angiography is currently considered an established technique for noninvasive evaluation of the coronary lumen as well as coronary plaques (8). However, MSCT assessment of the previously stented coronary artery is limited due to metal artifacts. Because of its radiolucent, polylactide backbone, the Absorb scaffold does not affect computed tomography (CT) image interpretation, and MSCT could be used to assess changes in the lumen and vessels after Absorb implantation. Furthermore, noninvasive fractional flow reserve (FFR) derived from MSCT was recently shown to be feasible with high diagnostic performance for the detection and exclusion of flow-limiting coronary lesions that cause ischemia, which might further refine the quality of the noninvasive follow-up (9).

We hereby report the 5-year clinical results, the luminal measurement, and noninvasive FFR assessment by MSCT in the original cohort of patients treated with an Absorb scaffold in the ABSORB Cohort A trial.

Methods

Study design. The design of this study was previously reported (3). Briefly, in this single-arm, prospective, open-label study, with safety and imaging endpoints, 30 patients were enrolled at 4 participating sites between March and July 2006. Patients were older than 18 years of age with a diagnosis of stable, unstable, or silent ischemia. All treated lesions were single, de novo in a native coronary artery of 3.0 mm, <8 mm for the 12-mm scaffold or ≤14 mm for the 18-mm scaffold (only 2 patients received an 18-mm scaffold), with a percentage of diameter stenosis ≥50% and <100% with a Thrombolysis In Myocardial Infarction flow grade of ≥1. Major exclusion criteria were patients presenting with an acute myocardial infarction (MI), unstable arrhythmias, or a left ventricular ejection fraction <30%, restenotic lesions, lesions located in the left main coronary artery, lesions involving a side branch >2 mm in diameter, and the presence of thrombus or another clinically significant stenosis in the target vessel. A risk analysis of multimodality imaging based on previously published reports was provided to the local ethics committees (10,11). The ethics committees approved the protocol at the participating institutions, and the enrolled patients gave written informed consent before inclusion. Four patients received a non-Absorb BVS metallic stent in addition to the study device. Clinical endpoints were assessed at 30 days, 6 and 9 months, and 1, 2, 3, 4, and 5 years. Noninvasive MSCT imaging studies were planned at 5 years. All major cardiac adverse events (MACE) were adjudicated by an independent clinical

From the *Department of Cardiology, Thoraxcenter, Erasmus Medical Center, Rotterdam, the Netherlands; †Jagiellonian University, Krakow, Poland; ‡Skejby Sygehus, Aarhus University Hospital, Skejby, Denmark; §Department of Radiology, Thoraxcenter, Erasmus Medical Center, Rotterdam, the Netherlands; ‖Cardialysis, Rotterdam, the Netherlands; and the ¶Auckland City Hospital, Auckland, New Zealand.

events committee, and a data safety monitoring board monitored patient safety.

Study device. The study device, the description of the polymers, and in vitro and pre-clinical data have been described elsewhere (3). The polymeric device consists of a backbone of poly-L-lactide (PLLA) coated with poly-D,L-lactide (PDLLA) that contains and controls the release of the antiproliferative drug everolimus. The long chains of PLLA and PDLLA are progressively shortened as ester bonds between lactide repeat units are hydrolyzed. Ultimately, PLLA and PDLLA fully degrade to lactic acid that is metabolized via the Krebs cycle to H_2O and CO_2. In vivo, small particles <2 mm in diameter are phagocytosed by macrophages.

Scaffolding procedure. The Absorb BVS was implanted after mandatory pre-dilation. When additional treatment was required, the Cypher sirolimus-eluting stent (Cordis, Miami, Florida) was used because there were no animal/pre-clinical data on overlapping Absorb BVS devices available at the time of patient enrollment. All patients were required to receive aspirin ≥75 mg/day for the study duration (5 years) and clopidogrel 75 mg/day for a minimum of 6 months.

MSCT angiography. CT scanners from all major manufacturers were used, including 64-slice CT (Brilliance 64, Philips, Best, the Netherlands; CVi, GE Healthcare, Milwaukee, Wisconsin), 256-slice CT (iCT, Philips), 320-slice CT (Aquilion One, Toshiba, Nasu, Japan), 64-slice dual-source CT (Definition, Siemens AG, Forchheim, Germany), and 128-slice dual-source CT (Definition Flash, Siemens). Standard acquisition techniques were used, which included beta-blockers in patients with a fast heart rate, tube settings depending on patient size (80 to 140 kV), and axial scan protocols for patients with lower heart rates to reduce radiation doses, all at the discretion of the individual sites. Images were reconstructed using thin slices (0.5 to 0.67 mm) and medium smooth reconstruction filters, including 1 or several phases depending on the scan protocol. All data were stored on a DVD for core laboratory evaluation.

MSCT analysis. The CT data were analyzed on a dedicated workstation (Multi-Modality Workstation, Siemens AG) using a validated cardiovascular analysis package (Circulation, Siemens AG) (12). Semiautomatically, a center lumen line was created through the treated coronary branch after which cross-sectional views of the vessel were reconstructed at ∼1-mm longitudinal steps, including the 5 mm proximal and distal to the device, using the platinum indicators as landmarks. Automatic segmentation of the vessel lumen, with manual correction was performed to measure the lumen area. The outer vessel borders were manually traced to approximate the total vessel size, using fixed window display settings: level, 750 Hounsfield units; width, 250 Hounsfield units. The mean, minimal, and maximal lumen areas within the treated lesion were determined for each slice. The
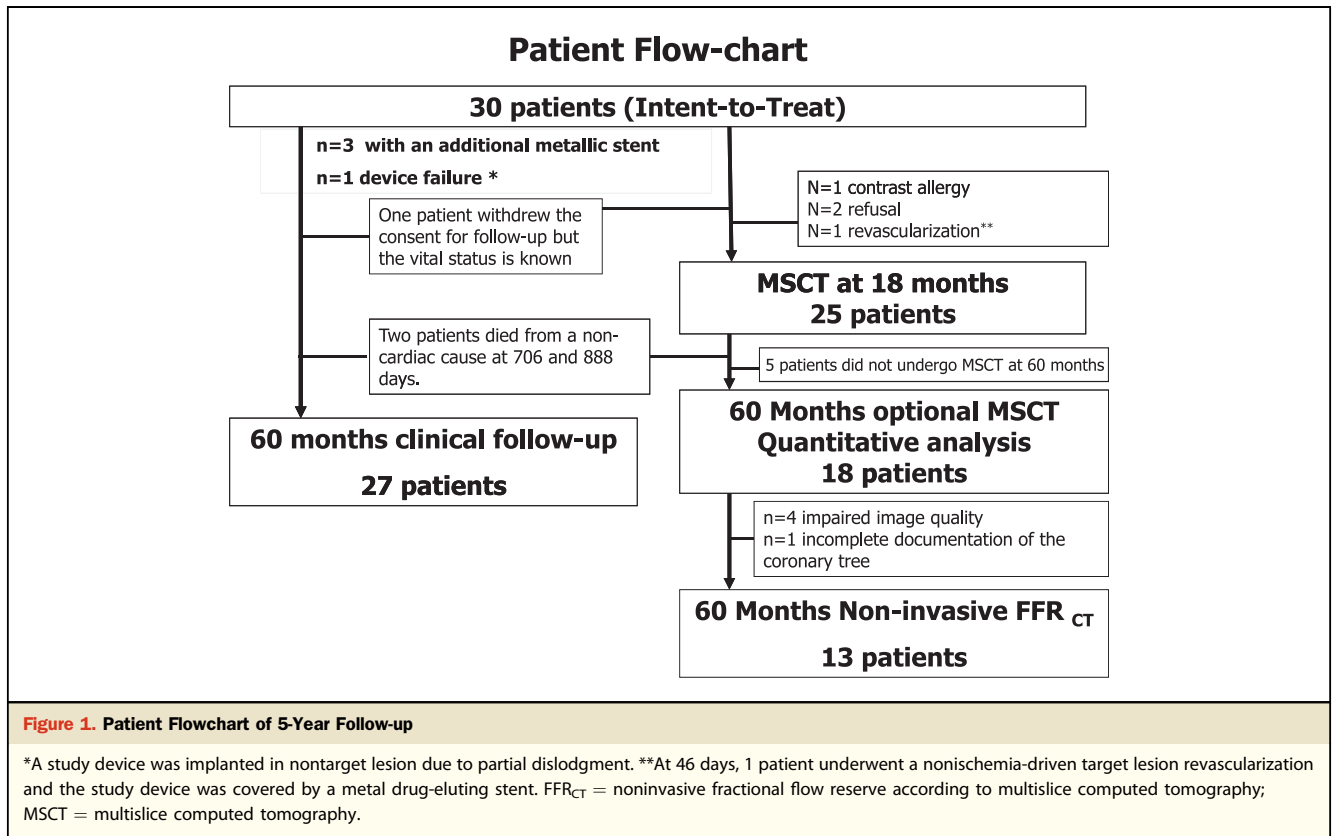
reference vessel lumen area was calculated as the average of the mean proximal and mean distal vessel areas. The lumen area stenosis was calculated as the reference minus the minimal lumen area as a percentage of the reference lumen area. In case of an ostial lesion or overlapping conventional stents, the reference lumen diameter was based on measurements of the opposite end only. Significant area stenosis was defined as 75%, which approximates a 50% diameter stenosis. Each cross section was qualitatively assessed for the presence of noncalcified plaque, calcified plaque, and mixed plaque (13–15). The percentage of cross sections of each plaque type was calculated as a number of cross sections with the plaque type divided by the total number of cross sections analyzed in the scaffolded segment. The interobserver reproducibility of minimum lumen area showed a Pearson correlation of 0.84 with an interclass correlation coefficient for absolute difference of 0.84 (interclass correlation coefficient for concordance of 0.91). The mean ± SD of the difference between observers was −0.96 ± 0.97 mm^2.

MSCT-based FFR assessment. The noninvasive FFR according to MSCT (FFR_{CT}) was performed in a blinded fashion by the independent core laboratory at HeartFlow, Inc. (Redwood City, California). The detailed methodology is described elsewhere (9). The FFR_{CT} technology is based on 3 key principles. Because patients with rest angina were excluded, the first is that coronary supply meets myocardial

Table 1. Baseline Characteristics

	Intention-to-Treat Population (N = 30)
Age, yrs	62 (54–70)
Male	18 (60)
Current smokers	6 (20)
Diabetes	1 (3)
Hypertension requiring medication	18 (60)
Hyperlipidemia requiring medication	19 (63)
Previous target vessel intervention	3 (10)
Previous myocardial infarction	1 (3)
Stable angina	21 (70)
Unstable angina	8 (27)
Silent ischemia	1 (3)
Target vessel	
Left anterior descending artery	15 (47)
Left circumflex artery	9 (30)
Right coronary artery	7 (23)
AHA/ACC lesion classification, %	
B1	60
B2	40
Mean reference vessel diameter, mm	2.60 (2.36–3.02)
Minimal lumen diameter, mm	1.01 (0.87–.22)
Diameter stenosis, %	58 (52–70)
Lesion length, mm	8.16 (6.04–10.96)

Values are median (interquartile range) and n (%).
AHA/ACC = American Heart Association/American College of Cardiology.

Patient Flow-chart

30 patients (Intent-to-Treat)

n=3 with an additional metallic stent
n=1 device failure *

One patient withdrew the consent for follow-up but the vital status is known

N=1 contrast allergy
N=2 refusal
N=1 revascularization**

**MSCT at 18 months
25 patients**

Two patients died from a non-cardiac cause at 706 and 888 days.

5 patients did not undergo MSCT at 60 months

**60 months clinical follow-up

27 patients**

**60 Months optional MSCT
Quantitative analysis
18 patients**

n=4 impaired image quality
n=1 incomplete documentation of the coronary tree

**60 Months Non-invasive FFR$_{CT}$

13 patients**

Figure 1. Patient Flowchart of 5-Year Follow-up

*A study device was implanted in nontarget lesion due to partial dislodgment. **At 46 days, 1 patient underwent a nonischemia-driven target lesion revascularization and the study device was covered by a metal drug-eluting stent. FFR$_{CT}$ = noninvasive fractional flow reserve according to multislice computed tomography; MSCT = multislice computed tomography.

demand at rest. Adherence to this principle enabled calculation of total resting coronary flow relative to ventricular mass (16,17). The second principle is that resistance of the microcirculation at rest is inversely but not linearly proportional to the size of the feeding vessel (18–23). The third principle is that microcirculation reacts predictably to maximal hyperemic conditions in patients with normal coronary flow (24). On the basis of these principles, a lumped parameter model representing the resistance to flow during simulated hyperemia was applied to each coronary branch of the segmented cardiac CT angiography model. The FFR$_{CT}$ was modeled for conditions of adenosine-induced hyperemia. The FFR$_{CT}$ core laboratory scientists were instructed as to the location of the scaffold within a coronary artery.

Three-dimensional models of the coronary tree and ventricular myocardium were reconstructed with custom methods applied to blinded cardiac CT angiography data for simulation of coronary flow and pressure. Blood was modeled as a Newtonian fluid with incompressible Navier-Stokes equations and solved subject to appropriate initial and boundary conditions with a finite element method on a parallel supercomputer (25). Because coronary flow and pressure are unknown a priori, a method to couple grouped parameter models of the microcirculation to the

outflow boundaries of the 3-dimensional model was used (26–28).

Definitions. The composite clinical endpoint is cardiac death, MI classified as Q-wave and non–Q-wave MI, and ischemia-driven (ID) target lesion revascularization (TLR). ID TLR implies revascularization at the target lesion, irrespective of the time window for angiographic control at 6 months or 2 years, associated with: 1) a positive functional ischemia study; 2) ischemic symptoms and angiographic minimal lumen diameter stenosis $\geq$50% by core laboratory quantitative coronary angiography (QCA); or 3) revascularization of a target lesion with a diameter stenosis $\geq$70% by core laboratory QCA without either ischemic symptoms or a positive functional study. For a diagnosis of non–Q-wave MI, elevation of creatine kinase levels $\geq$2 times the upper limit of normal with increased creatine kinase–myocardial band was required. Scaffold thrombosis was adjudicated according to the Academic Research Consortium definitions (29). Other clinical endpoints include all-cause mortality, non-ID TLR, and ID or non-ID target vessel revascularization (TVR).

Statistical analysis. For binary variables, percentages were calculated. For continuous variables, the median and interquartile range were computed. For imaging assessment, truly serial analysis is presented in tables and paired comparisons

Table 2. Hierarchical Major Adverse Cardiac Events Up to 5 Years

	6 Months (n = 30)	12 Months (n = 29)*	2 Yrs (n = 29)*	5 Yrs (n = 29)*
Cardiac death	0.00	0.00	0.00	0.00
Noncardiac death	0.00	0.00	3.4 (1.0)	6.9 (2.0)
MI				
Q-wave	0.00	0.00	0.00	0.00
Non–Q-wave	3.3 (1.0)†	3.4 (1.0)†	3.4 (1.0)†	3.4 (1.0)†
Cardiac death or MI	3.3 (1.0)†	3.4 (1.0)†	3.4 (1.0)†	3.4 (1.0)†
Ischemia-driven TLR				
By PCI	0.00	0.00	0.00	0.00
By CABG	0.00	0.00	0.00	0.00
Ischemia-driven MACE	3.3 (1.0)*	3.4 (1.0)*	3.4 (1.0)*	3.4 (1.0)*
Nonischemia-driven TLR	3.3 (1.0)†	3.4 (1.0)†	3.4 (1.0)†	3.4 (1.0)†
Nonischemia-driven TVR (non-TLR)	10.0 (3.0)	10.3 (3.0)	10.3 (3.0)	10.3 (3.0)
Any TVR‡	10.0 (3.0)	10.3 (3.0)	10.3 (3.0)	10.3 (3.0)
Stroke/TIA	0.00	0.00	0.00	0.00

Values are % or % (n). *One patient withdrew consent from the study after 6 months, but the patient's vital status remains available through the referring physician. †This patient also underwent a TLR, not qualified as ischemia-driven TLR (diameter stenosis = 42%) followed by post-procedural troponin qualified as non–Q-wave MI and died of Hodgkin's disease at 888 days post-procedure. ‡Any TVR includes both ischemia-driven and nonischemia-driven TVR.

CABG = coronary artery bypass graft; MACE = major adverse cardiac events; MI = myocardial infarction; PCI = percutaneous coronary intervention; TIA = transient ischemic attack; TLR = target lesion revascularization; TVR = target vessel revascularization.

between 18 months and 5 years were done by a Wilcoxon signed rank test. The p values presented in this paper are exploratory analyses only and should therefore be interpreted cautiously. All statistical analyses were performed with SPSS software version 18.0 (IBM, Armonk, New York).

Role of funding source. This study was sponsored by Abbott Vascular. The sponsor was involved in the design and conduct of the study and the collection, management, initial analysis, and interpretation of the data and had the right to a nonbinding review of the manuscript. Full monitoring ensured accuracy of data collection. Before the end of the 5-year follow-up, the protocol was amended to allow the patients who had undergone an MSCT scan as an optional investigation at 18 months to be re-consented to undergo a second MSCT scan at 60 months.

Results

Patient demographic data and a flow chart are shown in Table 1 and Figure 1, respectively. One patient withdrew consent from the study after the first 6 months of follow-up but the vital and clinical status of this patient remained available through the referring physician. Two patients died of a noncardiac cause during follow-up, and 5-year clinical follow-up was obtained in the remaining 27 patients. In 29 patients with any available follow-up, the median duration of follow-up was 1,862 days.

Hierarchical event rates concerning ID MACE are presented in Table 2. Up to 5 years, there was only 1 non–Q-wave MI related to the non-ID TLR of a nonflow-limiting stenosis (QCA diameter stenosis, 42%) of an Absorb at 46 days post-procedure (3,4,30,31). Two patients died of a noncardiac cause: 1 of Hodgkin's disease at 888 days and the other of a duodenal perforation at 706 days. In the entire cohort, there was no instance of scaffold thrombosis according to either the protocol or Academic Research Consortium definitions or a retrospective analysis requested by the U.S. Food and Drug administration at the end of 2006 for the assessment of on-/off-label use of the first-generation drug-eluting metal stents (29).

In addition to the patient described who experienced non-ID TLR at 46 days, 2 patients experienced a non-ID TVR. At 106 days post-procedure, in 1 patient experiencing angina at rest, an ergonovine test performed during recatheterization disclosed a dynamic subtotal occlusion (vasospasm) of the segment proximal to the scaffold; the patient received a 3.5 × 22-mm paclitaxel-eluting stent proximal to the scaffolded segment. At 5 years, the patient presented with recurrent angina and underwent MSCT follow-up that revealed a minimal lumen area of 2.0 mm^2 but with a negative noninvasive FFR$_{CT}$ of 0.87, whereas the intermediate branch had a significant stenosis with a positive FFR$_{CT}$ of 0.72 (Fig. 2). On day 1,780, invasive angiography showed a patent scaffolded segment (%diameter stenosis 35%) and a stenosed intermediate branch that was treated with a 2.5 × 18-mm metallic everolimus-eluting stent (ID TVR). The other patient who had received an Absorb in the distal left anterior descending artery received a metal drug-eluting stent in a moderate, nonsignificant stenosis (QCA %DS <50%) in the left anterior descending artery far proximal to the patent Absorb scaffold on day 85 (30,31).

The protocol mandated a minimum of 6 months of combined antiplatelet therapy but the actual duration was left to the discretion of the investigators who, in general, followed the guidelines of the European Society of Cardiology/American College of Cardiology/American Heart Association for antiplatelet use after metal drug-eluting stent implantation (32,33). At 1 year, 15 patients were receiving dual antiplatelet therapy, but only 1 patient remained on clopidogrel therapy at 5 years (Fig. 3). This patient restarted clopidogrel due to the repeat percutaneous coronary intervention in the nontarget lesion of the intermediate branch while the scaffolded segment was patent (Fig. 2).

Quantitative MSCT at 60 months compared with results at 18-months. At 5 years, 18 patients underwent MSCT as an optional investigation that was performed at 3 of 4 centers (Figs. 1 and 4). Quantitative analysis of the scaffolded segment was feasible in all patients (Table 3). All scaffolds were patent, with a median minimal lumen area of 3.25 mm^2 (interquartile range [IQR]: 2.20 to 4.33 mm^2) as
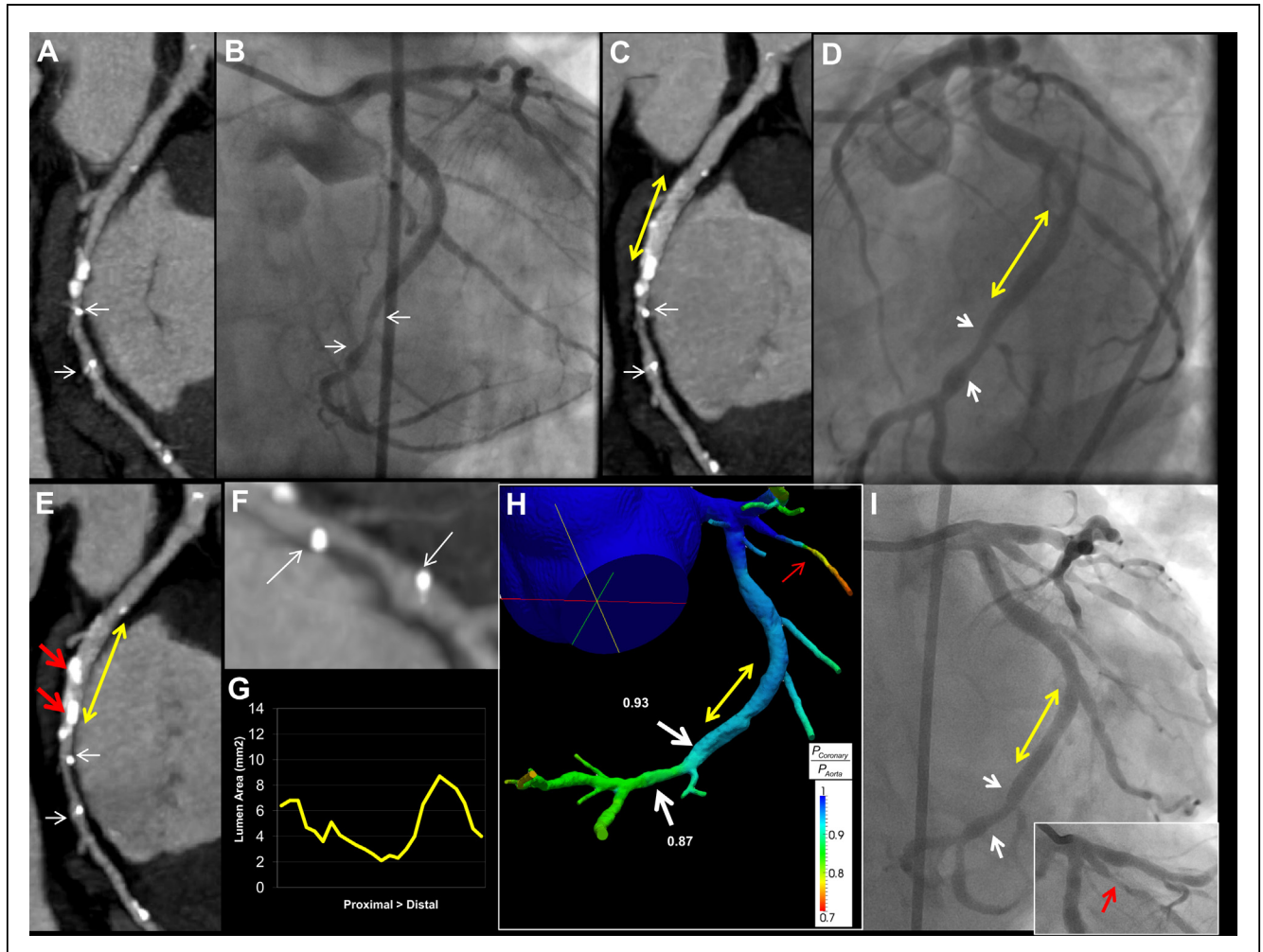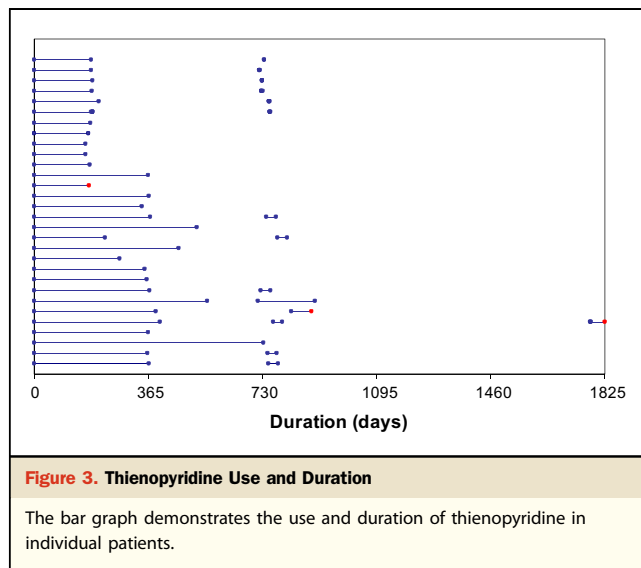
Figure 2. A Case of Non-ID TVR

The patient received an Absorb 3 12-mm scaffold in the distal left circumflex artery. **(A)** Multislice computed tomography (MSCT) post-procedure. **(B)** Angiography post-procedure. **(C, D)** The patient received a 3.5 × 22-mm paclitaxel-eluting stent (visible on 18-month MSCT [**yellow arrow**]) proximal to the scaffolded segment as a treatment of a pharmacologically induced vasospasm. The scaffolded segment was patent at 2-year angiographic follow-up. At 5 years, the patient presented with recurrent angina and underwent MSCT follow-up. The maximal intensity projection of the left circumflex artery showed the patent scaffolded segment with intermediate stenosis (between **white arrows**, **E and F**) and increased deposition of calcium **(red arrows, E)** in the previously implanted metal stents **(yellow arrow, E)**. Quantitative analysis showed a minimum lumen area of 2.0 mm^2 suggesting a possibly significant stenosis **(G)**; however, the noninvasive fractional flow reserve was negative with a value of 0.87 **(H)**. Angiography showed a patent scaffolded segment (%diameter stenosis 35%) and a stenosed intermediate branch **(I, red arrow)** that was considered as a culprit lesion. TVR = target vessel revascularization.

well as 33.3% median area stenosis (IQR: 12.8% to 43.8%) (Figs. 5 and 6). The lumen volume on average was 72.12 mm^3 at 18 months and 73.85 mm^3 at 60 months. At the proximal edge, the MSCT measurement remained numerically unchanged. In the distal segment, the vessel area decreased significantly from 18 months to 60 months (Δ −0.70 mm^2, p = 0.03), which could be largely attributed to the numerical decrease in plaque area (Δ−0.47 mm^2, p = 0.25) because the lumen area remained stable (Δ 0.01 mm^2, p = 1.0). In the scaffolded segment, some similar trends in remodeling and plaque decrease were observed, although the 4 area measurements did not show statistically significant change. The frequency of

noncalcified and calcified plaque did not change from 18 months to 60 months.

Noninvasive FFR$_{CT}$ results at 60 months. Of 18 patients, noninvasive FFR analysis was feasible in 13. In 4 patients, severe artifact hindered FFR analysis, whereas in 1 case, FFR could not be calculated due to incomplete documentation of the entire coronary tree. The FFR distal to the scaffolded segment was a median 0.86 (IQR: 0.82 to 0.94).

Figure 7 shows the relationship between minimal area and noninvasive FFR distal to the scaffolded segment of the treated vessel. The methodology also enables the practitioner to assess the FFR continuously along each vessel of the coronary circulation. The evaluation of the relationship was

Figure 3. Thienopyridine Use and Duration

The bar graph demonstrates the use and duration of thienopyridine in individual patients.

therefore also performed between minimal lumen area and the change in FFR between the proximal and distal parts of the scaffold landmarked by the 2 radiopaque markers (Fig. 7). There were 3 asymptomatic patients with an FFR_{CT} between 0.75 and 0.80.

Discussion

This report on 5-year clinical outcomes of the first-in-humans ABSORB trial demonstrates a low ID MACE rate of 3.4% (1 patient) without any scaffold thrombosis, early, late, or very late. The serial noninvasive quantitative MSCT assessment was feasible with an option of functionality assessment and demonstrated that the lumen and vessel dimensions were unchanged from 18 months to 5 years.

According to the protocol, 5-year follow-up is the last follow-up of this first-in-humans study conducted for the phase II trial of the everolimus-eluting bioresorbable scaffold. Instead of performing invasive follow-up, noninvasive follow-up with MSCT was optionally performed at 3 of 4 centers for the following reasons: at the time of writing the protocol in 2005, it already appeared challenging to plan 2 angiographic follow-ups at 6 and 24 months for purely scientific reasons, and 5-year invasive follow-up was not planned. The invasive imaging of IVUS and OCT at 2 years demonstrated the beneficial effects of the device such as late lumen enlargement with restoration of vasoreactivity, which renders difficult the justification of an additional invasive follow-up at 5 years. In addition, the 2-year QCA was actually limited in 19 of 30 patients because 11 patients either withdrew their consent or refused the repeat invasive imaging at 2 years, whereas MSCT at 18 months was available for 25 patients (4). We therefore decided not to

perform invasive imaging of IVUS and OCT but rather to repeat MSCT imaging that could be performed non-invasively and could provide enough information on the evolution of the wall thickness and lumen from 18 months to 60 months.

The trial confirmed the feasibility of noninvasive functional and anatomic assessment of the scaffold, a fact that opens new avenues for noninvasive control of the patency of treated coronary lesions. Currently some manufacturers have increased the radiopacity of their metal struts by using a new radiopaque alloy such as platinum, facilitating the acute positioning and deployment of the device but rendering the assessment of the patency by noninvasive MSCT problematic (1,34).

The serial assessment of the lumen by MSCT revealed the persistence of the lumen area up to 5 years after the everolimus-eluting bioresorbable scaffold implantation with a nonsignificant decrease in plaque area, which could be the result of dissolution and incorporation of the polylactide struts into the vessel wall. Pre-clinical data showed a completion of polylactide mass loss (i.e., bioresorption) of 70% and 100% at 18 months and at 2 years, respectively. However, OCT can still image the strut as a black box at 2 years, but on histology, the polylactide polymeric strut has already been bioresorbed and is replaced by proteoglycan. At 3 and 4 years, the strut void has been filled in with the connective tissue replacing proteoglycan, which results in shrinkage of strut void on histology. The decrease in plaque area observed in the current analysis may therefore reflect this integration process after bioresorption between 2 and 5 years, although the resolution of the MSCT technique and the small number of observation do not allow statistical significance to be reached.

Coronary atherosclerosis is a continuous disease process and necessitates preventive measures and intensive pharmacological treatment. Indeed, after bioresorption of the polymer, the vessel and the lumen are able to change dynamically in response to physiological stimuli, biological environment, and pharmacological treatment due to the absence of a permanent metal endoluminal prosthesis (35). This emphasizes the importance of treating the underlying atherosclerotic process after a bioresorbable scaffold implantation. It should be underscored that in the absence of a metal structure, restenosis after scaffolding can be treated with another scaffold without any of the complexities of treating classic in-stent restenosis within a metal stent. In the near future, scaffolding, in theory, could be applied after appropriate preparation of the stenotic lesion using the classic tools of the interventional cardiologist such as rotablators, cutting balloons, laser, high-pressure balloons, and others.

The FFR_{CT} has been validated against invasive FFR in 2 multicenter trials, demonstrating that the technology has a good correlation with an invasive FFR and adds more
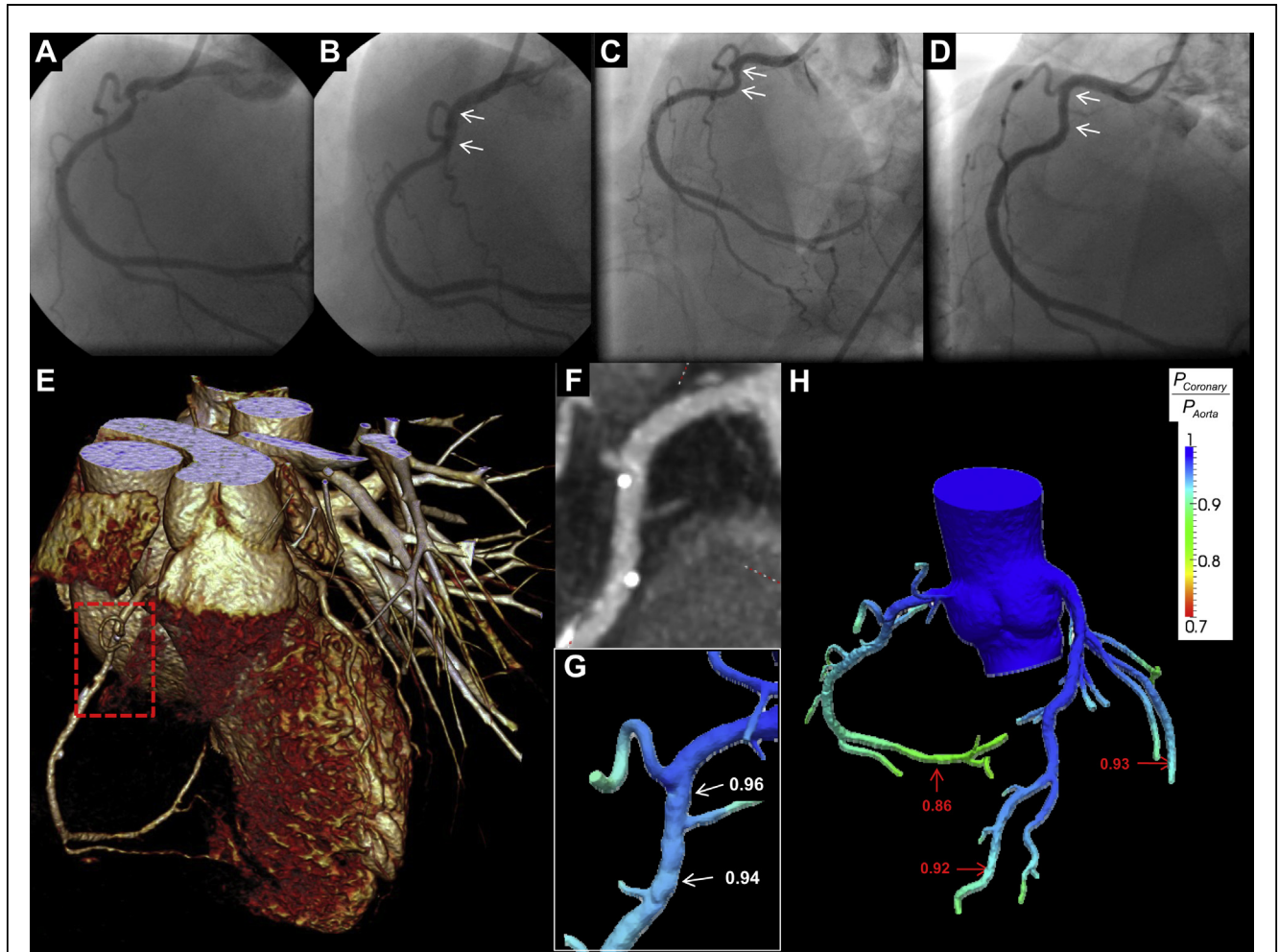
Figure 4. A Case Example of 5 Year MSCT Follow-up

The patient had a short stenotic lesion in the proximal right coronary artery **(A)** that was successfully treated by a 3 × 12-mm Absorb Bioresorbable scaffold **(white arrows in B)**. At 6 months **(C)** and 2 years **(D)**, angiographic follow-up was performed to demonstrate the patent scaffolded segment **(white arrows)**. At 5 years, multislice computed tomography (MSCT) follow-up was performed and demonstrated a patent scaffolded segment **(red rectangle** in volume rendering image in **E)**. In maximal intensity projection **(F)**, the metal markers indicating both ends of the scaffold remained visible as white dots on MSCT 5 years after implantation. MSCT was further processed for assessment of noninvasive fractional flow reserve (FFR), which demonstrated the absence of functionally significant stenosis in the proximal and distal segments of the scaffolded segment **(G**, 0.96 and 0.94, respectively). The noninvasive FFR also proved the absence of any significant stenosis in all major epicardial vessels **(H**, distal right coronary artery, 0.86; distal left anterior descending artery, 0.92; distal left circumflex artery, 0.93).

accuracy on diagnosis of coronary artery disease compared with quantitative MSCT (9,36). In the current study, the feasibility of quantitative assessment of coronary MSCT was 100%, whereas the noninvasive FFR assessment was possible in 72%. Good image quality of all coronary arteries and low heart rate are mandatory for noninvasive FFR because the 3-dimensional modeling of the entire coronary tree is indispensable for flow simulation. For quantitative assessment of the lumen, the image quality of the nonscaffolded segment is technically less demanding because the imaging protocol only focused on the scaffold area. Due to the post-hoc assessment of MSCT acquisition, no specific investigational requirement such as a low heart rate was prospectively

recommended to the investigators. The feasibility of FFR$_{CT}$ could, in the near future, be improved as the image is acquired optimally and the imaging technology further advanced.

The computational algorithms used in the FFR$_{CT}$ analysis provide highly reproducible results well within the precision of measured FFR. Of note, published reports demonstrate that FFR$_{CT}$ accuracy is less affected by MSCT image quality than CT stenosis (37). Regarding the short- (5 min) or medium- (1 h) term reproducibility, radiation and patient safety concerns have precluded repeat MSCT studies on the same patient to investigate such reproducibility of the image data acquisition as historically assessed for

Table 3. Serial Quantitative MSCT Assessment at 18 Months and 5 Years

	18 Months	5 Yrs	Difference (5 Yrs − 18 Months)	p Value
Proximal segment, mm^2 (n = 15)				
Minimal lumen area	4.70 (3.30 to 5.30)	4.80 (3.10 to 6.20)	−0.10 (−0.50 to 1.40)	0.31
Mean lumen area	5.82 (3.78 to 6.52)	5.85 (4.12 to 7.50)	0.10 (−0.58 to 0.78)	0.60
Mean vessel area	12.80 (10.80 to 18.00)	12.70 (11.60 to 15.00)	0.40 (−2.60 to 2.00)	1.0
Mean plaque area	7.02 (6.58 to 10.62)	6.85 (6.00 to 9.13)	−0.10 (−1.84 to 1.68)	0.93
Distal segment, mm^2 (n = 16)				
Minimal lumen area	4.15 (2.35 to 5.00)	3.45 (2.65 to 4.90)	0.10 (−0.80 to 1.10)	0.92
Mean lumen area	4.97 (3.22 to 5.69)	4.56 (3.08 to 5.96)	0.01 (−0.68 to 0.90)	1.0
Mean vessel area	11.90 (8.80 to 15.40)	11.40 (8.30 to 13.60)	−0.70 (−1.70 to 0.00)	0.03
Mean plaque area	7.49 (5.60 to 9.75)	5.79 (4.69 to 8.33)	−0.47 (−2.07 to 0.48)	0.25
Scaffolded segment, mm^2 (n = 18)				
Minimal lumen area	3.10 (2.10 to 3.80)	3.25 (2.20 to 4.30)	0.20 (−0.20 to 0.90)	0.21
Mean lumen area	4.47 (3.36 to 5.58)	4.29 (3.38 to 5.73)	0.36 (−0.08 to 0.62)	0.11
Mean vessel area	13.17 (10.35 to 15.93)	11.93 (9.00 to 16.47)	−0.31 (−1.63 to 0.54)	0.26
Mean plaque area	8.23 (6.98 to 11.18)	7.10 (5.44 to 10.14)	−1.31 (−2.23 to 0.81)	0.23
Mean reference area	5.23 (3.62 to 6.08)	5.29 (3.47 to 6.30)	−0.08 (−0.45 to 0.80)	0.76
Area stenosis, %	31.6 (25.6 to 45.8)	33.3 (13.2 to 40.7)	−2.3 (−10.8 to 2.0)	0.25
Cross sections with noncalcified plaque, %	100 (52.9 to 100.0)	87.5 (33.3 to 100.0)	0.0 (−8.9 to 0.0)	0.12
Cross sections with mixed plaque, %	0 (0 to 43.8)	6.25 (0 to 56.3)	0.0 (0.0 to 4.8)	0.37
Cross sections with calcified plaque, %	0 (0 to 0)	0 (0 to 0)	0 (0 to 0)	0.50
FFR$_{CT}$ (n = 13)				
Proximal		0.91 (0.88 to 0.96)		
Distal		0.86 (0.82 to 0.94)		
Δ (distal FFR$_{CT}$ − proximal FFR$_{CT}$)		−0.03 (−0.05 to −0.02)		

Values are median (interquartile range).

FFR$_{CT}$ = noninvasive fractional flow reserve according to multislice computed tomography; MSCT = multislice computed tomography.

quantitative coronary angiography (38). Patient preparation, contrast timing, and scan technique would be expected to affect the quality and reproducibility of the resultant images.

Study limitations. This first-in-humans trial included only patients with a single and simple anatomic lesion in a population in which a majority of patients presented with
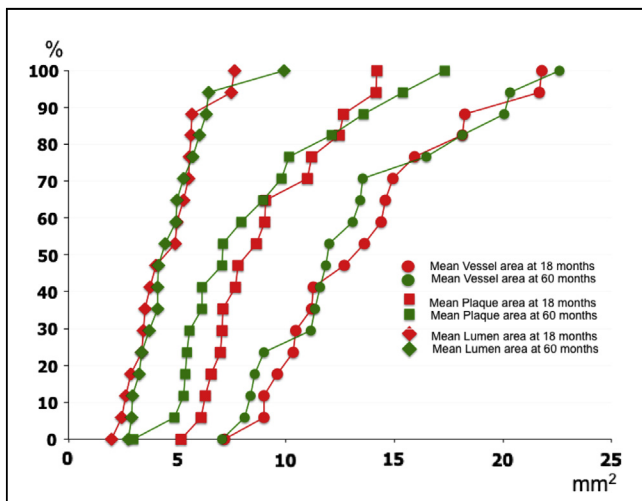
Figure 5. Cumulative Frequency Distribution Curves of Mean Lumen Area, Plaque Area, and Vessel Area at 18 Months and 5 Years

All frequency distribution curves as assessed by multislice computed tomography.
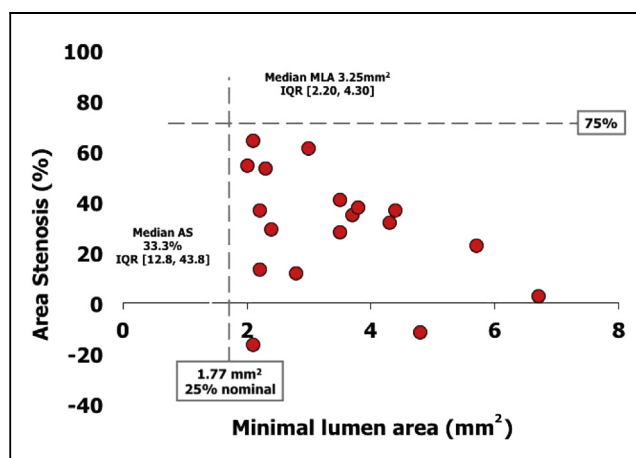
Figure 6. MLA Versus Area Stenosis in the Scaffolded Segment (n = 18)

The median of minimal lumen area and area stenosis was 3.25 mm^2 (IQR: 2.20 to 4.30) and 33.3% (IQR: 12.8 to 43.8), respectively. The **dashed lines** indicate 75% area stenosis and 25% of nominal area. Nominal area is the theoretical area of a scaffold of 3.0 mm (e.g., 7.07 mm^2). AS = area stenosis; IQR = interquartile range; MLA = minimal lumen area.
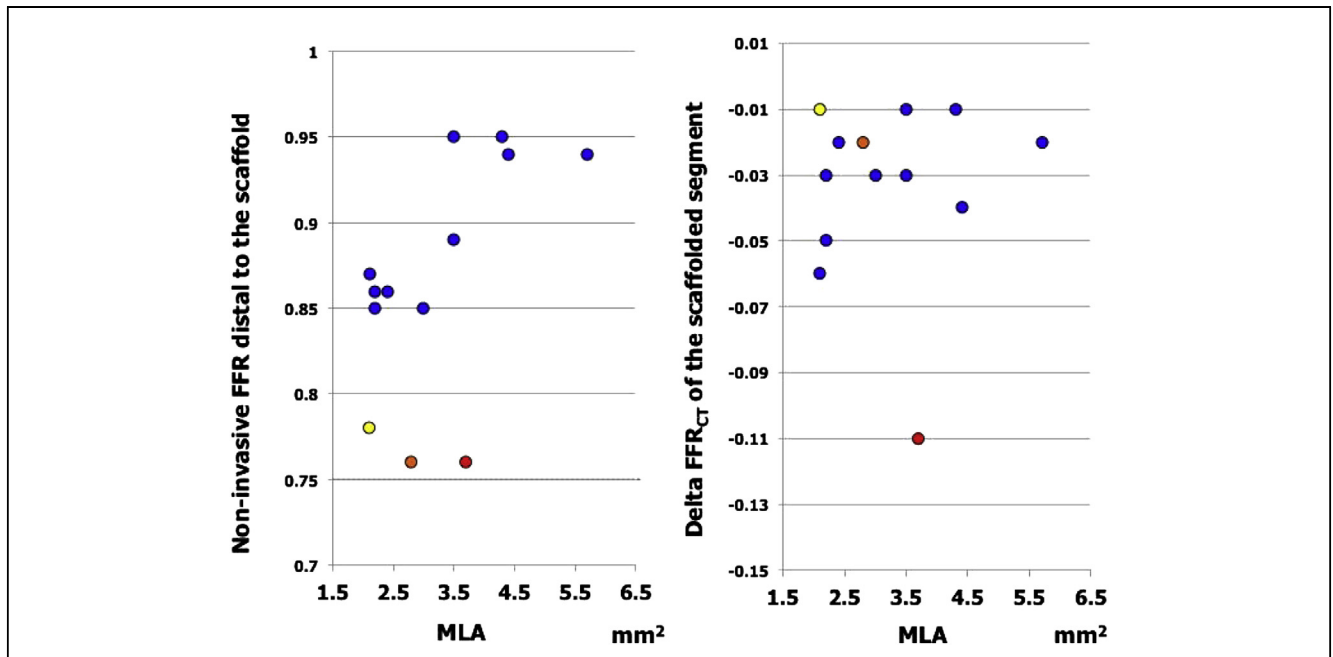
Figure 7. Minimum Lumen Area Versus Noninvasive FFR

(Left) A scatterplot of 5-year noninvasive FFR$_{CT}$ immediately distal to the scaffold versus quantitative MLA in the scaffold segment assessed by multislice computed tomography (MSCT) (n = 13). **(Right)** A scatterplot of the change in FFR$_{CT}$ across the scaffolded segment (distal FFR$_{CT}$ − proximal FFR$_{CT}$) versus MLA. There were 3 asymptomatic patients with a FFR$_{CT}$ value between 0.75 and 0.80. In 2 patients, MSCT revealed an intermediate stenosis at least 5 mm proximal to the scaffolded segment, whereas the scaffolded segments showed no flow-limiting stenoses with a minimal FFR$_{CT}$ gradient of −0.01 and −0.02 **(right, yellow and orange dots)**. The third patient **(red dot)** had diffuse disease with a FFR$_{CT}$ of 0.71 in the distal segment of the left anterior descending artery. According to the investigational protocol of this center, the patient underwent a diagnostic angiography by catheterization, during which an invasive FFR showed a progressive, nonlocalized pressure gradient in the diffusely diseased left anterior descending artery. Due to the absence of focal flow-limiting stenosis, the asymptomatic patient was kept under medical treatment. FFR = fractional flow reserve; FFR$_{CT}$ = noninvasive fractional flow reserve according to multislice computed tomography; MLA = minimal lumen area.

stable angina. Although the standard MSCT acquisition techniques were used, the scan protocol was adjusted for different MSCT scanners used at each institution and each follow-up at the discretion of individual sites. To control the acquisition quality, however, the sites were asked twice, at 18 and 60 months, to send test run MSCT data to the MSCT core laboratory for review of protocol compliance and data quality. The small numbers of patients followed by noninvasive angiography is more related to the optional character of the investigation than to the lack of technical feasibility. So far, the clinical validation of this new methodological approach has only been obtained in 1 clinical trial and awaits further validation.

Conclusions

The low event rate at 5 years suggests sustained safety after the implantation of a fully bioresorbable Absorb everolimus-eluting scaffold. Noninvasive assessment of the coronary artery after treatment with this device is feasible, with the possibility of simultaneous functional assessment in selected cases.

REFERENCES

1. Otsuka M, Tanimoto S, Sianos G, et al. "Radio-lucent" and "radio-opaque" coronary stents characterized by multislice computed tomography. Int J Cardiol 2009;132:e8–10.
2. Eggebrecht H, Rodermann J, Hunold P, et al. Images in cardiovascular medicine. Novel magnetic resonance-compatible coronary stent: the absorbable magnesium-alloy stent. Circulation 2005;112:e303–4.
3. Ormiston JA, Serruys PW, Regar E, et al. A bioabsorbable everolimus-eluting coronary stent system for patients with single de-novo coronary artery lesions (ABSORB): a prospective open-label trial. Lancet 2008; 371:899–907.

4. Serruys PW, Ormiston JA, Onuma Y, et al. A bioabsorbable ever-olimus-eluting coronary stent system (ABSORB): 2-year outcomes and results from multiple imaging methods. Lancet 2009;373:897–910.

5. Tanimoto S, Serruys PW, Thuesen L, et al. Comparison of in vivo acute stent recoil between the bioabsorbable everolimus-eluting coronary stent and the everolimus-eluting cobalt chromium coronary stent: insights from the ABSORB and SPIRIT trials. Catheter Cardiovasc Interv 2007;70:515–23.

6. Tanimoto S, Bruining N, van Domburg RT, et al. Late stent recoil of the bioabsorbable everolimus-eluting coronary stent and its relationship with plaque morphology. J Am Coll Cardiol 2008;52:1616–20.

7. García-García HM, Gonzalo N, Pawar R, et al. Assessment of the absorption process following bioabsorbable everolimus-eluting stent implantation: temporal changes in strain values and tissue composition using intravascular ultrasound radiofrequency data analysis. A substudy of the ABSORB clinical trial. EuroIntervention 2008;4:443–8.

8. Voros S, Rinehart S, Qian Z, et al. Prospective validation of stan-dardized, 3-dimensional, quantitative coronary computed tomographic plaque measurements using radiofrequency backscatter intravascular ultrasound as reference standard in intermediate coronary arterial lesions: results from the ATLANTA (assessment of tissue characteris-tics, lesion morphology, and hemodynamics by angiography with frac-tional flow reserve, intravascular ultrasound and virtual histology, and noninvasive computed tomography in atherosclerotic plaques) I study. J Am Coll Cardiol Intv 2011;4:198–208.

9. Koo BK, Erglis A, Doh JH, et al. Diagnosis of ischemia-causing coronary stenoses by noninvasive fractional flow reserve computed from coronary computed tomographic angiograms. Results from the prospective multicenter DISCOVER-FLOW (Diagnosis of Ischemia-Causing Stenoses Obtained Via Noninvasive Fractional Flow Reserve) study. J Am Coll Cardiol 2011;58:1989–97.

10. Jang IK, Bouma BE, Kang DH, et al. Visualization of coronary atherosclerotic plaques in patients using optical coherence tomography: comparison with intravascular ultrasound. J Am Coll Cardiol 2002;39:604–9.

11. Nissen SE, Gurley JC, Grines CL, et al. Intravascular ultrasound assessment of lumen size and wall morphology in normal subjects and patients with coronary artery disease. Circulation 1991;84:1087–99.

12. Leber AW, Johnson T, Becker A, et al. Diagnostic accuracy of dual-source multi-slice CT-coronary angiography in patients with an inter-mediate pretest likelihood for coronary artery disease. Eur Heart J 2007; 28:2354–60.

13. Voros S, Rinehart S, Qian Z, et al. Coronary atherosclerosis imaging by coronary CT angiography: current status, correlation with intravascular interrogation and meta-analysis. J Am Coll Cardiol Img 2011;4:537–48.

14. Raff GL, Abidov A, Achenbach S, et al. SCCT guidelines for the interpretation and reporting of coronary computed tomographic angi-ography. J Cardiovasc Comput Tomogr 2009;3:122–36.

15. Lehman SJ, Schlett CL, Bamberg F, et al. Assessment of coronary plaque progression in coronary computed tomography angiography using a semiquantitative score. J Am Coll Cardiol Img 2009;2:1262–70.

16. West GB, Brown JH, Enquist BJ. A general model for the origin of allometric scaling laws in biology. Science 1997;276:122–6.

17. Steele BN, Olufsen MS, Taylor CA. Fractal network model for simu-lating abdominal and lower extremity blood flow during resting and exercise conditions. Comput Methods Biomech Biomed Eng 2007;10:39–51.

18. Murray CD. The physiological principle of minimum work: I. The vascular system and the cost of blood volume. Proc Natl Acad Sci U S A 1926;12:207–14.

19. Hutchins GM, Miner MM, Boitnott JK. Vessel caliber and branch-angle of human coronary artery branch-points. Circ Res 1976;38:572–6.

20. Kamiya A, Togawa T. Adaptive regulation of wall shear stress to flow change in the canine carotid artery. Am J Physiol 1980;239:H14–21.

21. Zarins CK, Zatina MA, Giddens DP, Ku DN, Glagov S. Shear stress regulation of artery lumen diameter in experimental atherogenesis. J Vasc Surg 1987;5:413–20.

22. Zhou Y, Kassab GS, Molloi S. On the design of the coronary arterial tree: a generalization of Murray's law. Phys Med Biol 1999; 44:2929–45.

23. Zhou Y, Kassab GS, Molloi S. In vivo validation of the design rules of the coronary arteries and their application in the assessment of diffuse disease. Phys Med Biol 2002;47:977–93.

24. Wilson RF, Wyche K, Christensen BV, Zimmer S, Laxson DD. Effects of adenosine on human coronary arterial circulation. Circulation 1990;82:1595–606.

25. Kim HJ, Vignon-Clementel IE, Figueroa CA, Jansen KE, Taylor CA. Developing computational methods for three-dimensional finite element simulations of coronary blood flow. Finite Elements Anal Design 2010;46:514–25.

26. Müller J, Sahni O, Li X, Jansen KE, Shephard MS, Taylor CA. Anisotropic adaptive finite element method for modelling blood flow. Comput Methods Biomech Biomed Engin 2005;8:295–305.

27. Sahni O, Müller J, Jansen KE, Shephard MS, Taylor CA. Efficient anisotropic adaptive discretization of the cardiovascular system. Comput Methods Appl Mech Engrg; 2006:5634–55.

28. Kim HJ, Vignon-Clementel IE, Coogan JS, Figueroa CA, Jansen KE, Taylor CA. Patient-specific modeling of blood flow and pressure in human coronary arteries. Ann Biomed Eng 2010;38:3195–209.

29. Cutlip DE, Windecker S, Mehran R, et al. Clinical end points in coronary stent trials: a case for standardized definitions. Circulation 2007;115:2344–51.

30. Dudek D, Onuma Y, Ormiston JA, Thuesen L, Miquel-Hebert K, Serruys PW. Four-year clinical follow-up of the ABSORB ever-olimus-eluting bioresorbable vascular scaffold in patients with de novo coronary artery disease: the ABSORB trial. EuroIntervention 2012;7:1060–1.

31. Onuma Y, Serruys PW, Ormiston JA, et al. Three-year results of clinical follow-up after a bioresorbable everolimus-eluting scaffold in patients with de novo coronary artery disease: the ABSORB trial. EuroIntervention 2010;6:447–53.

32. Silber S, Albertsson P, Aviles FF, et al. Guidelines for percutaneous coronary interventions. The Task Force for Percutaneous Coronary Interventions of the European Society of Cardiology. Eur Heart J 2005; 26:804–47.

33. Smith SC Jr., Feldman TE, Hirshfeld JW Jr., et al. ACC/AHA/SCAI 2005 guideline update for percutaneous coronary intervention: a report of the American College of Cardiology/American Heart Association Task Force on Practice Guidelines (ACC/AHA/SCAI Writing Committee to Update the 2001 Guidelines for Percutaneous Coronary Intervention). J Am Coll Cardiol 2006;47:e1–121.

34. Hamon M, Champ-Rigot L, Morello R, Riddell JW. Diagnostic accuracy of in-stent coronary restenosis detection with multislice spiral computed tomography: a meta-analysis. Eur Radiol 2008;18:217–25.

35. Serruys PW, Garcia-Garcia HM, Onuma Y. From metallic cages to transient bioresorbable scaffolds: change in paradigm of coronary revascularization in the upcoming decade? Eur Heart J 2012;33:16–25b.

36. Min JK, Leipsic J, Pencina MJ, et al. Diagnostic accuracy of frac-tional flow reserve from anatomic CT angiography. JAMA 2012;308:1237–45.

37. Min JK, Koo BK, Erglis A, et al. Effect of image quality on diagnostic accuracy of noninvasive fractional flow reserve: results from the prospective multicenter international DISCOVER-FLOW study. J Cardiovasc Comput Tomogr 2012;6:191–9.

38. Reiber JH, Serruys PW, Kooijman CJ, et al. Assessment of short-, medium-, and long-term variations in arterial dimensions from computer-assisted quantitation of coronary cineangiograms. Circulation 1985;71:280–8.

Key Words: bioresorbable scaffold ■ everolimus ■ multislice computed tomography ■ noninvasive functional assessment.